Polymers & biopolymers

Temperature-dependent electrowetting behavior on Teflon AF1600

Yijie Xiang[1,*] , Paul Fulmek[1], Daniel Platz[1], and Ulrich Schmid[1]

[1] *Institute of Sensor and Actuator Systems, TU Wien, Gusshausstr. 27–29, 1040 Vienna, Austria*

ABSTRACT

In the growing application field of electrowetting (EW), reliable control of the wetting behavior by an applied voltage is required over a wide temperature range. Despite the rising interest of EW, only few data are reported in the literature on the EW behavior as a function of temperature. In this paper, we investigate the quasi-static EW response on one of the most widely used hydrophobic materials, Teflon AF1600, in a temperature range from 25 to 70 °C. The contact angle versus voltage is analyzed to illustrate the EW behavior. The results are in good agreement with the friction-adsorption model, which explains the contact angle (CA) hysteresis by a temperature-independent friction-like force and a temperature-dependent contribution of liquid adsorption onto a dielectric surface. The EW-CAs show a small asymmetry with respect to the polarity of the applied voltage, which might be due to the temporary and reversible charge trapping on the dielectric layer. The results underline that the different effects of the temperature-independent friction force and the temperature-dependent adsorption need to be taken into account to predict and control the CA in any EW-based application scenario.

Springer

GRAPHICAL ABSTRACT

Increasing voltage $\qquad$ Decreasing voltage
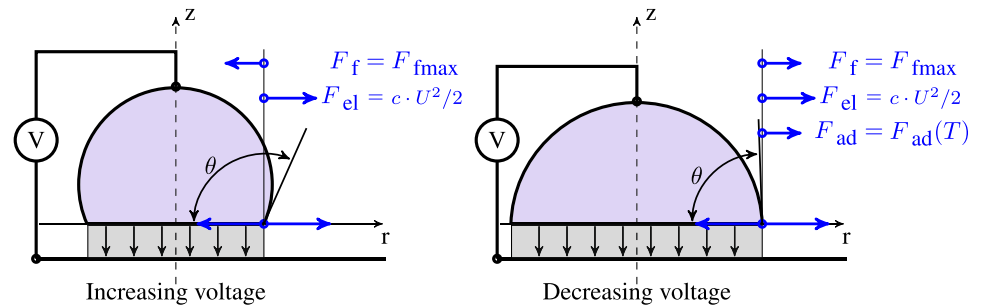
Introduction

Electrowetting-on-dielectrics (EWOD) is one of the most wide-spread techniques for controlling the contact angle (CA) between an electrolyte droplet and a dielectric surface due to the low energy consumption, as well as easy and fast manipulation of small liquid volumes [1]. In the classical EWOD experimental setup an electrically conductive liquid droplet is placed on a plane, dielectric layer above an electrode. In static equilibrium, the electrically conductive liquid represents a constant electric potential, especially the base surface is an equipotential surface representing an electrode with a defined area. The dielectric-electrolyte contact angle is determined by the respective interface energies and the electric energy stored in the solid dielectric layer. Based on the benefits of EWOD, EWOD has been widely used in applications, for example, generating transporting and mixing small droplets in microfluidic devices [2–4], adjustable liquid lenses [4–9], etc. Different CAs are measured since the static CA can vary due to material and ambient-related factors, such as surface roughness [10], chemical inhomogeneity [11], adsorption and temperature [12, 13]. The maximal CA difference is defined as the CA hysteresis [14–16]. Several works have been published to explore the EW response on materials with high CA hysteresis [15, 17, 18]. In these studies, the EW response was investigated for increasing and decreasing droplet

volume in order to achieve the advancing and receding triple-line, and the respective CA. Compared to the theoretical predictions, not only the advancing and receding EW-CAs have been observed [15, 17], but also a completely different behavior of the triple-line, namely stick-slip behavior, has appeared [18]. Those results indicate that the triple-line movement direction, which determines whether a droplet is in advancing or receding CA state, plays an important role in the determination of EW-CA, and needs to be taken into account for predicting the actuation performance within the EW-based applications. Furthermore, the CA is affected by temperature [13, 19], especially in the liquid lens application field, since the interface tensions as well as the CA hysteresis are temperature-dependent [13, 20]. Therefore, a deeper understanding of the EW-CA dependence on temperature is required to enable a precise prediction and control of the wetting properties.

In this work, we present an experimental setup to determine the quasi-static EW-CA under isothermal condition at temperatures ranging from 25 to 70 °C. We investigate the EW response on Teflon AF1600 based on the friction-adsorption (FA) model, which is concluded from our previous work [13]. This model describes the CA hysteresis by introducing a temperature-independent friction force and a temperature-dependent contribution of water adsorption onto Teflon AF1600.

Materials and methods

Fabrication of samples

A silicon (Si) wafer, with an electrical bulk resistivity of 0.015–0.025 Ω cm and a thickness of $325 \pm 15 \mu$m is used as substrate. The Si wafer is firstly cleaned with buffered hydrofluoric acid 87.5 wt% NH_4F, 12.5 wt% HF) for 2 min to remove the native oxide. Titanium and gold layers with the thickness of 50 nm and 150 nm are thermally evaporated on one side of the Si wafer as electrode. Then, the sample is annealed in vacuum at 280 °C for 24 h to enhance the ohmic contact between the Si wafer and the electrode layer. On the other side of the Si wafer, a titanium primer is deposited by spin-coating at 4000 rpm for 1 min (spin coater, Süß Technic) and annealed at 120 °C for 2 min, to enhance the adhesion of Teflon AF1600. Next, 4 wt% Teflon AF1600 (DuPont Co.) in fluorinert FC-40 solvent (3M Company) is spun with 1000 rpm for 120 s and annealed first at 175 °C for 10min, substantially at 165 °C for 5 min [13, 21]. Finally, the wafer is cut into 15×15 mm samples for the EW experiments. The thickness 1091 ± 15 nm of the Teflon AF1600 film was determined by measuring the step height with a profilometer (Dektak 8). The surface roughness was determined by atomic force microscope (AFM, Bruker Dimension Edge) and resulted in a mean root square roughness $R_{RMS} = 0.82$ nm (with a maximum roughness $R_{max} = 8.19$ nm) on a scan area of $10 \times 10 \mu$m^2. The dielectric constant of the Teflon AF1600 layer is experimentally determined by an additionally evaporated gold electrode on top of the Teflon AF, $\varepsilon_r = 1.92$, independent of the magnitude and polarity of the voltage in the range between -100 and $+100$ V, more experimental details and results are shown in Supplementary Information.

Experimental setup

The experimental setup consists of a drop shape analyzer (DSA, Krüss DSA30S, software Advance) and a custom-built temperature controlled test chamber (Fig. 1). Images taken by DSA with a resolution of 200 pixel/mm are analyzed for the droplet contour, to determine the contact angle with a resolution of $0.01°$ and an accuracy of $0.1°$. The test chamber consists of a massive Al cover and a solid aluminum (Al) base plate with a platinum resistance thermometer (Pt100) as integrated temperature

sensor. The temperature at the Al base plate is precisely controlled ($\Delta T < 0.01$ °C) by a temperature controller (Meerstetter TEC-1091) connected to the Peltier element. Additionally, two resistance heaters and a K-type sensor control the temperature of the cover ($\Delta T < 0.5$ °C). The high thermal conductivity of the Al minimizes any temperature gradients in the chamber. The small hole in the cover allows inserting both deposition needle and platinum needle for the electrical connection, and the pressure balance with respect to the ambient atmosphere.

A droplet of saline water, (mixing of DI water, 16–18 $M\Omega$ cm, and saline water) with a size of 8–10 μL is created on the needle and then deposited on the Teflon AF1600 surface after applying a cleaning procedure with acetone and isopropanol, and drying with nitrogen gas. The Al base plate is surrounded by a groove which is filled with water to adjust the humidity to prevent droplet volume loss. The evolution of the droplet volume over time inside the experimental chamber has been observed, the volume loss rate is less then 4 nL/min. We therefore neglect the influence of volume changes on the CA in this work. The bottom electrode (shown in Fig. 1) is connected to the electrical ground potential, whereas the platinum (Pt) wire is used to apply voltage to the conductive droplet.

The CA is determined by the tangential fit method, where the curvature of the contour line around the triple-line is determined, and the CA is found as the angle between the tangent and the surface. With this local fit method, the insertion of the Pt electrode has no influence on the CA calculation. The electrical voltage is in the range of ± 80 V to prevent permanent and irreversible changes in surface properties due to CA saturation (70–72° at 88 V), and is supplied by a pair of Kepco amplifiers (BOP), controlled by a function generator (Agilent 33220A). We have chosen symmetrical triangular voltages with constant slopes well below the quasi-static limit to perform our EWOD experimental series. Details about the calculation of the quasi-static limit can be seen in Supplementary Information.

Friction-adsorption model description

The classical Young–Lippmann (YL) equation describes the CA (θ) in dependence of the voltage U applied at the dielectric layer [3]:

$$\cos \theta = \cos \theta_Y + \frac{c \cdot U^2}{2 \cdot \gamma_{la}}, \tag{1}$$

where c (F/m^2) is the specific capacitance of the dielectric layer. θ_Y is the CA described by Young's equation [22], as the result of the force equilibrium of surface tensions, γ_{sa}, γ_{la} and γ_{sl} (N/m), at the triple-line:

$$\cos \theta_Y = \frac{\gamma_{sa} - \gamma_{sl}}{\gamma_{la}}, \tag{2}$$

the subscripts s, l, a representing solid, liquid, and surrounding air, respectively.

An explanation for the CA hysteresis has been recently proposed by the authors [13], by introducing additional force components arising from friction and adsorption at the solid dielectric surface to the classical Young's equation. The static CA is determined by the three interface tensions, γ_{sl}, γ_{la} and γ_{sa}, a friction-like force F_f, and a contribution of adsorption on the dielectric surface F_{ad}, shown in Fig. 2. The vectorial force equilibrium at the triple-line reduces to the equilibrium of the horizontal r-components, while the vertical z-components are compensated by the substrate. With the additional force F_{el} due to the stored electric energy,

$$F_{el} = c \cdot U^2/2, \tag{3}$$

the CA, θ, is described by:

$$\gamma_{la} \cdot (\cos \theta - \cos \theta_Y) = F_f + F_{ad} + F_{el}. \tag{4}$$

In the initial, static equilibrium state ($F_f = F_{ad} = F_{el} = 0$), Eq. (4) gives the standard Young's CA, θ_Y [Eq. (2)]. While the sign of the forces F_{el} and F_{ad} is always positive, indicating the direction of increasing base diameter in case of nonzero value, the friction force F_f is in the range from $-F_{fmax}$ to $+F_{fmax}$, which can act in both directions. Values of F_{fmax} (3.15 mN/m) and the temperature-dependent adsorption contribution $F_{ad}(T)$ have been experimentally determined for Teflon AF layers by the authors recently [13]. The temperature-dependent $F_{ad}(T)$ is written as a linear approximation in the investigated temperature range between 25 and 70 °C by:

$$F_{ad}(T) = F_{25} \cdot (1 - \alpha \cdot (T - T_{25})), \tag{5}$$

with the parameter values $F_{25} = 4.95$ mN/m, $\alpha = 0.0182(1/K)$, and $T_{25} = 25$ °C.

The temperature dependence of $\theta_Y(T)$ can be approximated according to the authors' previous work as [13]:

$$\cos \theta_Y(T) = -\frac{\beta}{\gamma_{la}(T)}, \tag{6}$$

with the parameter $\beta = 37.15$ mN/m and the temperature-dependent liquid-air interface tension $\gamma_{la}(T)$ [23]. Equation (6) is well justified for temperatures lower than 50 °C and is used as an approximation at higher temperature in this work as well. More details about Eq. (6) can be found in Supplementary Information.

The applied voltage creates an additional force F_{el}, which is compensated by the friction force up to its maximum value F_{fmax} in the direction against F_{el}. Further increasing the F_{el} ($\propto U^2$) will move the triple-line towards the dry dielectric surface with $F_{ad} = 0$. The advancing CA is then described by:

$$\gamma_{la} \cdot \cos \theta = \gamma_{la} \cdot \cos \theta_Y - F_{fmax} + F_{el}. \tag{7}$$

When the F_{el} is decreased from the applied voltage level, the triple-line tends to move over the dielectric surface previously covered by the droplet. The force equilibrium is established by the variable friction force F_f ($-F_{fmax} \leq F_f \leq + F_{fmax}$) and by the adsorption contribution F_{ad}. The receding CA is therefore written as:

$$\gamma_{la} \cdot \cos \theta = \gamma_{la} \cdot \cos \theta_Y + F_{ad} + F_{fmax} + F_{el}. \tag{8}$$

Figure 3a summarizes the solutions of Eqs. (7) and (8) and illustrates the advancing and receding CA, and the CA hysteresis. The CA hysteresis is defined as the CA difference between the advancing and the receding limit, the static CA can assume any value within these limits. The vertical lines in Fig. 3b show the range of the CA hysteresis during EW for constant voltages, e.g., due to changes in the droplet volume. In this work, however, the droplet volume is constant, any CA variation is caused by the applied voltage. Figure 3c shows the CA behavior for a positive voltage half-cycle: for an increasing applied voltage, the CA stays constant until reaching the advancing CA limit. In this constant CA regime, the force equilibrium is established additionally by the variable F_f and the increasing F_{el} [see Eq. (4)]. Further increasing the voltage level drives the CA along the advancing line (blue line in Fig. 3), with the uniquely defined dependence $\theta(U)$ [Eq. (7)], accompanied by a
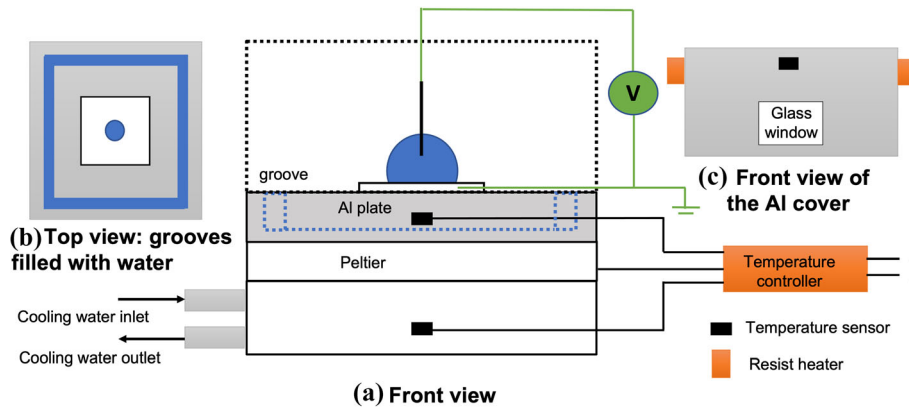
Figure 1 Illustration of the experimental setup [13]. **A** Front view. **B** Top view. **C** Front view of the Al cover with glass windows. A Peltier element under the Al plate, two resistance heaters at the Al cover (black dash line in A, details seen in C), temperature sensors and a temperature controller guarantee a homogeneous temperature contribution inside the chamber. Two glass windows in the cover (shown in C) are assembled to allow the illumination and observation. A small opening at the top of the cover allows inserting a needle to deposit the liquid droplet and a 0.1 mm diameter Platinum (Pt) needle for electrical connection. The groove (blue dash line in A, details seen in B) is filled with water to control the humidity and prevent droplet volume loss during experiments.

triple-line movement. When the voltage starts decreasing, the CA again stays constant as long as F_f and F_{ad} can compensate for the changing of F_{el}, until the receding CA limit is reached. From there on the CA follows the receding CA line (red line in Fig. 3), with $\theta(U)$ given by Eq. (8). For $U = 0$ V the maximum receding CA, θ_{rec}^{max}, is determined, which cannot be exceeded by any following voltage changes.

The influence of the temperature dependence $F_{ad}(T)$, $\theta_Y(T)$ and $\gamma_{la}(T)$ [Eqs. (5)–(8)] on the EW response will be presented in the next section.

Results and discussion

Characteristic EW response

Several EWOD experiments have been performed with ten cycles of a symmetric triangular voltage signal (shown in Fig. 4) with voltage slopes between 1 V/s and 16 and with the maximum amplitude 80 V.

The CA results $\theta(U)$ of the experiments at 30 °C are shown in Fig. 5 to compare the classical YL-equation to our FA approach, and prove the negligible influence of the used voltage slopes. Furthermore, the results show high accordance between experimental data and the FA model in the positive applied voltage range. In the negative voltage range, the CA is perfectly predicted by the FA model up to about −40 V. A larger negative voltage level leads to a higher CA

(1–3° at −80 V). This variation is observed in each cycle and is explained by charge trapping on the dielectric surface [24–26]. The trapping effect weakens the electrical field. As a consequence, the electrical energy stored in the layer is reduced, and the EW-CA is larger than expected at a given voltage level (Eq. (4)).

Temperature-dependent EW-CA

Further EW experiments are carried out with a voltage ramp speed of 10 V/s for ten cycles in a temperature range between 25 and 70 °C. As described in the previous part, we extracted characteristic EW-CA values for the chosen voltage amplitude: the minimal advancing CA, θ_{adv}^{min}, for both voltage polarities, $U = 80V$ and $U = -80$ V (blue points in Fig. 3a). The maximal receding CA, θ_{rec}^{max}, for zero voltage, $U = 0$ (red point in Fig. 3a). We compared the average values of θ_{adv}^{min} and θ_{rec}^{max} from the ten cycles to the EW-CA described by the YL equation and the FA model [Eqs. (7), (8)] over temperature, as shown in Fig. 6. The maximal receding CA, θ_{rec}^{max}, increases with temperature. At the temperatures lower than 50 °C the EW-CAs are consistent with the FA model (Fig. 6a). The EW-CAs at higher temperatures are overestimated by the FA model, and more scattered, as showing in the authors' previous work [13]. The average minimal advancing CA, θ_{adv}^{min}, determined by
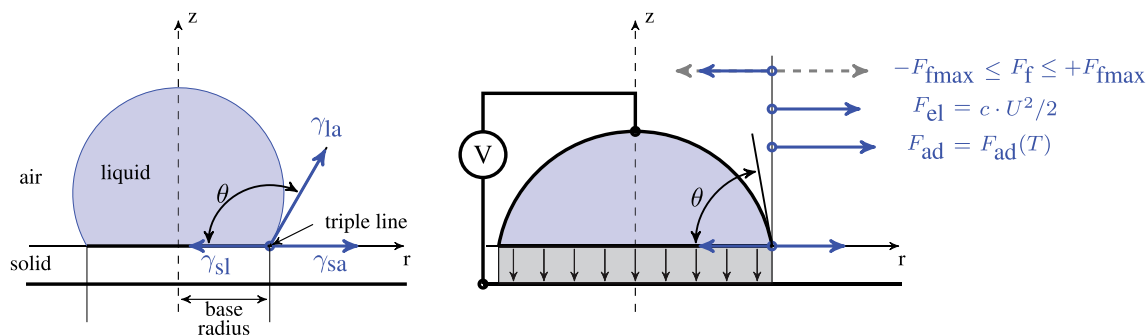
Figure 2 Static forces equilibrium at the triple-line. Left: Young's CA equilibrium of interface tensions. Right: additional forces due to friction F_f, adsorption F_{ad}, and the electric field energy F_{el}. The electric field energy is stored in the gray shaded area below the droplet.
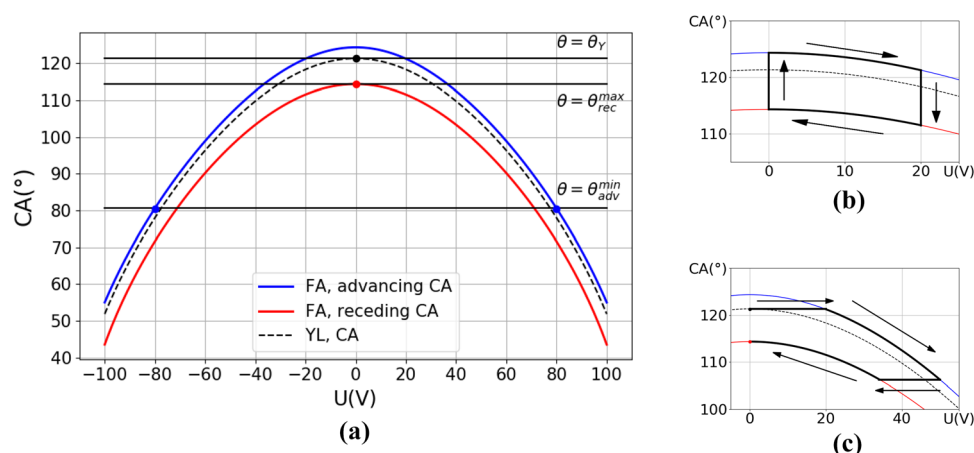

Figure 3 **a** Voltage dependence of the advancing (in blue) and the receding CA (in red) at temperature of $30\,^\circ$C according to the FA model. The limits of the friction-force F_f ($-F_{fmax} \le F_f \le +F_{fmax}$) and $F_{ad}(T)$ define the CA hysteresis range. The black point represents a droplet with θ_Y ($F_f = F_{ad} = F_{el} = 0$). The red point represents the maximal receding CA (θ_{rec}^{max}) at $U = 0$ V. The blue points represent the minimal advancing CA (θ_{adv}^{min}) at ± 80 V. **b** A sequence of CA variation is shown within the limits of the advancing and receding CA. For a given applied voltage, the CA can be manipulated e.g., by increasing or decreasing the droplet volume, shown by the vertical lines. **c** CA control by voltage: starting with $\theta = \theta_Y$ the increasing applied voltage (horizontal line) cannot influence the CA until the intersection with the advancing CA line (blue) is reached. Then, the EW-CA follows the advancing line $\theta(U)$ until the applied voltage level starts decreasing. A horizontal line describes the constant CA until the receding line (red) is reached when decreasing voltage. Then, the CA follows the receding line until $U = 0$ V, the maximum receding CA (θ_{rec}^{max}) is reached and determined, which cannot be exceeded by any following voltage changes.

Eq. (7), decreases with temperature, and this trend is consistent with the CA predicted by the FA model (Fig. 6b, c). However, the results for the negative voltage polarity show higher CAs by 1–3 °, in comparison to the experimental values for the positive voltage and the expected results from the FA model. The reason could be negative charge trapping onto the Teflon AF1600 layer [24–26]. This observed trapping effect is reversible since the CA at the positive voltage half-cycles is well predicted by the FA model over all applied ten cycles.

Conclusion

In this work, we investigated the quasi-static EW-CA in dependence of temperature and applied voltage. We successfully applied the friction-adsorption (FA) model to describe and explain the EW-CAs and the CA hysteresis. The experimental results and the model predictions are in good agreement. The results further show that CA variations, namely the variations of the forces parallel to the solid surface at the triple-line, are composed of two contributions: the temperature-independent friction-like force, and the
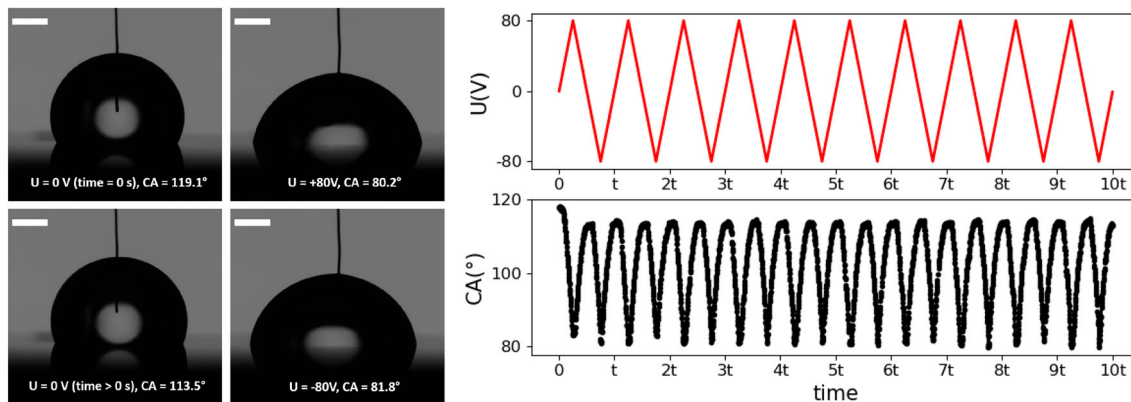
Figure 4 Left: corresponding images of the droplet at different applied voltage values. The length of the white bar represents 1 mm. Right: applied symmetric triangular voltage (in red) and the corresponding EW-CA (in black) over ten cycles at $T = 30\,°C$. The time axis is scaled using the period length $t = 32$ s.
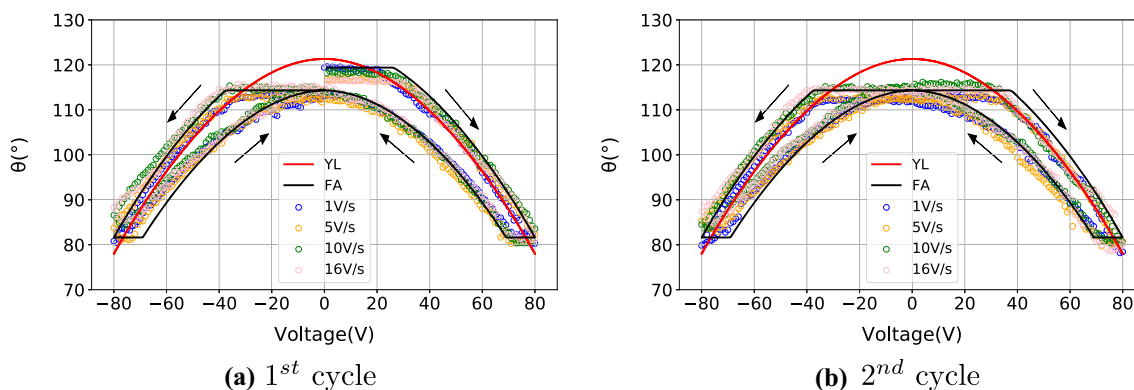

(a) 1st cycle

(b) 2nd cycle

Figure 5 Characteristic EW response at $T = 30\,°C$ with different voltage slopes for the first cycle (**a**), and the second cycle (**b**). The solid red line represents the EW-CA described by the classical YL equation [Eq. (2)]. The solid black line is the EW-CA described by the FA model [see Eqs. (7), (8)].

temperature-dependent adsorption of liquid molecules onto the solid dielectric surface. The friction force limit ($-F_{fmax}$) contributes to the determination of the advancing CA, while the friction force limit and adsorption ($+F_{fmax} + F_{ad}$) contribute to the calculation of the receding CA.

Moreover, the results in this work show and describe the important influence of temperature on the EW-CA. The available EW-CA range ($\theta_{rec}^{max} - \theta_{adv}^{min}$) by applying a maximal voltage 80V on a Teflon AF1600 layer (1091 ± 15 nm) changes with temperature by about $2.5°/10$ K. For EWOD-based applications, like adjustable liquid lenses, a temperature

control unit is encouraged to be implemented for a precise control and determination of EW-CA. In addition, our experiments show an influence of the voltage polarity on the CA. This effect could be due to the temporary and reversible charge trapping on the Teflon AF1600 surface.

In future work, we will further investigate the applicable range of the FA model, and extend it to other hydrophobic materials and liquids.

• Dielectric property characterization.
• Calculation of the quasi-static limit.
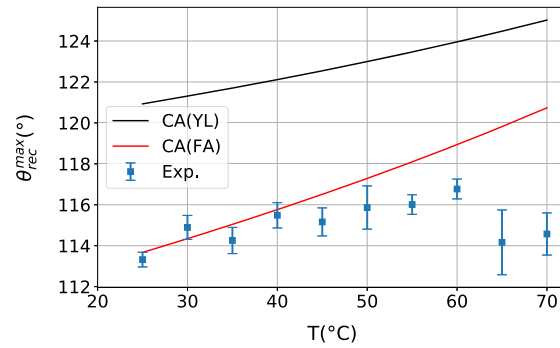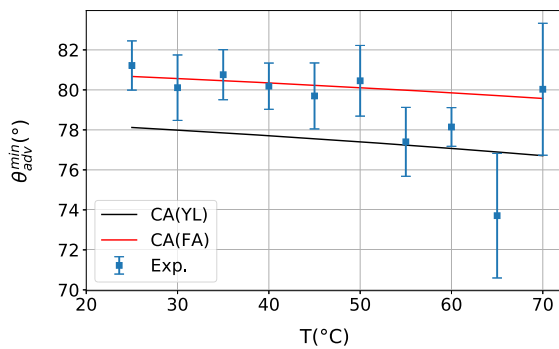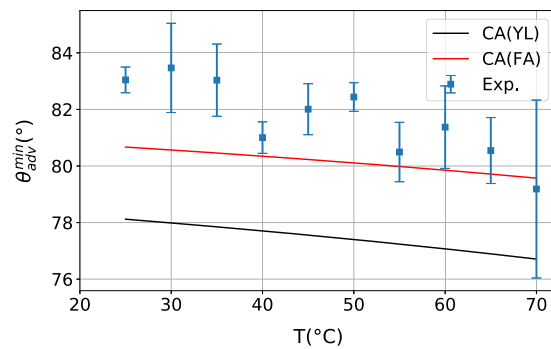• Details of the temperature-dependent θ_Y.

(a) $\theta_{\text{rec}}^{\max}$, $U = 0\,\mathrm{V}$

(b) $\theta_{\text{adv}}^{\min}$, $U = 80\,\mathrm{V}$.

(c) $\theta_{\text{adv}}^{\min}$, $U = -80\,\mathrm{V}$.

Figure 6 The characteristic EW-CAs with ramping speed of 10 V/s for ten cycles over temperature: **a** θ_{rec}^{max} for $U = 0\,\mathrm{V}$, **b** θ_{adv}^{min} for positive polarity $U = +80\,\mathrm{V}$, **c** θ_{adv}^{min} for negative polarity $U = -80\,\mathrm{V}$.

References

[1] Chen L, Bonaccurso E (2014) Electrowetting-from statics to dynamics. Adv Coll Interface Sci 210:2–12

[2] Jain V, Raj TP, Deshmukh R, Patrikar R (2017) Design, fabrication and characterization of low cost printed circuit

board based EWOD device for digital microfluidics applications. Microsyst Technol 23(2):389–397

[3] Mugele F, Baret J-C (2005) Electrowetting: from basics to applications. J Phys: Condens Matter 17(28):R705

[4] Li J et al (2020) Current commercialization status of electrowetting-on-dielectric (EWOD) digital microfluidics. Lab Chip 20(10):1705–1712

[5] Berge B, Peseux J (2000) Variable focal lens controlled by an external voltage: an application of electrowetting. Eur Phys J E 3(2):159–163

[6] Terrab S, Watson AM, Roath C, Gopinath JT, Bright VM (2015) Adaptive electrowetting lens-prism element. Opt Express 23(20):25838–25845

[7] Roques-Carmes T, Gigante A, Commenge J-M, Corbel S (2009) Use of surfactants to reduce the driving voltage of switchable optical elements based on electrowetting. Langmuir 25(21):12771–12779

[8] Lim WY, Supekar OD, Zohrabi M, Gopinath JT, Bright VM (2018) Liquid combination with high refractive index contrast and fast scanning speeds for electrowetting adaptive optics. Langmuir 34(48):14511–14518

[9] Huang H, Zhao Y (2019) Optofluidic lenses for 2d and 3d imaging. J Micromech Microeng 29(7):073001

[10] Quéré D (2008) Wetting and roughness. Annu Rev Mater Res 38:71–99

[11] Woodward J, Gwin H, Schwartz D (2000) Contact angles on surfaces with mesoscopic chemical heterogeneity. Langmuir 16(6):2957–2961

[12] Lam CN, Wu R, Li D, Hair M, Neumann A (2002) Study of the advancing and receding contact angles: liquid sorption as a cause of contact angle hysteresis. Adv Coll Interface Sci 96(1–3):169–191

[13] Xiang Y, Fulmek P, Platz D, Schmid U (2022) Temperature dependence of water contact angle on Teflon AF1600. Langmuir 38(4):1631–1637

[14] Eral HB, Mannetje DJCM, Oh JM (2013) Contact angle hysteresis: a review of fundamentals and applications. Coll Polym Sci 291(2):247–260

[15] Merrill MH, Reid RC, Gogotsi N, Thomas JP (2018) Electrowetting on polyimide and silicon substrates with high hysteresis. Microsyst Technol 24(12):4847–4854

[16] Joanny J, De Gennes P-G (1984) A model for contact angle hysteresis. J Chem Phys 81(1):552–562

[17] Li F, Mugele F (2008) How to make sticky surfaces slippery: contact angle hysteresis in electrowetting with alternating voltage. Appl Phys Lett 92(24):244108

[18] Reid RC, Merrill MH, Thomas JP (2020) Stick-slip behavior during electrowetting-on-dielectric: polarization and substrate effects. Microfluid Nanofluid 24(10):1–9

[19] Wadhai SM, Sawane YB, Banpurkar AG (2020) Electrowetting behaviour of thermostable liquid over wide temperature range. J Mater Sci 55(6):2365–2371

[20] Butt HJ, Kappl M (2010) Surface and interfacial forces. Wiley Online Library

[21] Chemours Company FC (2016) Teflon AF, Amorphous Fluoroplastic Resins. https://teflon-af-product-info.pdf. https://www.teflon.com

[22] Young T (1805) III. An essay on the cohesion of fluids. Philos Trans R Soc Lond 95:65–87

[23] Vargaftik N, Volkov B, Voljak L (1983) International tables of the surface tension of water. J Phys Chem Ref Data 12(3):817–820

[24] Wu H et al (2020) Electrically controlled localized charge trapping at amorphous fluoropolymer-electrolyte interfaces. Small 16(2):1905726

[25] Banpurkar AG et al (2017) Spontaneous electrification of fluoropolymer-water interfaces probed by electrowetting. Faraday Discuss 199:29–47

[26] Verheijen H, Prins M (1999) Reversible electrowetting and trapping of charge: model and experiments. Langmuir 15(20):6616–6620